13 June 2002

ELSEVIER

Chemical Physics Letters 359 (2002) 121–126

CHEMICAL PHYSICS LETTERS

www.elsevier.com/locate/cplett

Tungsten disulphide coated multi-walled carbon nanotubes

R.L.D. Whitby [a], W.K. Hsu [a], C.B. Boothroyd [b], H.W. Kroto [a], D.R.M. Walton [a,*]

[a] *School of Chemistry, Physics and Environmental Science, University of Sussex, Falmer, Brighton BN1 9QJ, UK*
[b] *Department of Materials Science and Metallurgy, University of Cambridge, Pembroke Street, Cambridge CB2 3QZ, UK*

Received 21 November 2001; in final form 18 April 2002

Abstract

Multi-walled carbon nanotubes (MWCNs), coated with ordered WS_2 mono- or multi-layers, are generated by pyrolysing H_2S/N_2 over MWCNs thinly coated with WO_3. High-resolution transmission electron microscopy (HRTEM) reveals the presence of hexagonal WS_2 arrays in the tube surface, consistent with the WS_2 simulated structure.

1. Introduction

Single-walled carbon nanotubes (SWCNs), unlike MWCNs, do not show (0 0 0 2) X-ray diffraction along the *c*-axis. Accordingly, the 3D ordering (e.g. $10\bar{1}1$ diffraction maxima) is absent from SWCNs, whereas the in-plane diffraction maxima (e.g. $10\bar{1}0$ and $11\bar{2}0$) remain [1]. The surface image of SWCNs, established by STM, reveals 0–30° chirality, and the measured $dI/dV - V_{bias}$ profile is consistent with the results of band theory, i.e. the local density of states [2,3]. Iijima estimates that in order to observe in-plane fringes for SWCNs by transmission electron microscopy (TEM), at least 4–5 C atoms must be aligned within a 0.2 nm thick wall parallel to the incident beam [4]. In the case of SWCNs, the diameter must be at least 1 nm. The electrons can be strongly or weakly scattered by the tubes [5]; strong scattering arises from the tube wall sections parallel with the incident beam (i.e. 0 0 2 fringes), and weak scattering from sections perpendicular to the incident beam. SWCNs only exhibit 0 0 0 2 basal plane fringes vertical to the tube axis in the TEM study. The hexagonal structure, located between the 0 0 0 2 side-wall fringes of a MWCN, has been observed previously by high-resolution transmission electron microscopy (HRTEM) [6–8]. It was concluded that hexagonal patterns arise from the basal planes perpendicular to the beam, when the individual C-shells in a MWCN have the same chirality [6]. Recently, C_{60} molecules, encapsulated in SWCNs, have been detected by HRTEM, which shows the presence of weak peapod-like fringes within the SWCNs [9]. The individual molecules are ca. 7 Å in diameter. It is noteworthy that although only 2–3 C-atoms are aligned within a 2 Å-wide section of the electron beam for C_{60}, they can still be clearly observed.

* Corresponding author. Fax: +44-1273-677196.
E-mail address: d.walton@sussex.ac.uk (D.R.M. Walton).

0009-2614/02/$ - see front matter
PII: S0009-2614(02)00667-X

Nanotubes consisting of W and S (or Mo and S) have been produced recently [10]. They also exhibit a hexagonal structure, but give rise to darker and thicker 0 0 0 2 side-wall HRTEM fringes than do carbon nanotubes, due to stronger scattering by W and S atoms. The in-plane lattice structure is actually a triple-layer stack i.e. S—W—S, (S—S distance is 3.2 Å) [11]. The difficulties in observing the in-plane hexagonal structure between 0 0 0 2 side-wall fringes of a multi-walled WS_2 nanotube by HRTEM are; firstly, the structural fringes are subject to strong interference from the adjacent WS_2 sheets [12]; secondly, a range of chiralities are probably present in multi-walled WS_2 nanotubes [13]; thirdly, these nanotubes frequently contain encapsulated WO_3 which obscures the fringes [14]. In order to minimise interference from the adjacent WS_2 layers, single-walled WS_2 nanotubes, free from other encapsulated material, are required. The well-established method of preparing multi-walled nanotubes involves $WO_3 \rightarrow WS_2$ conversion [15]. This route does not lend itself to WS_2 SWNT formation, as the smallest oxide particles (5 nm in diameter) will result in at least 3-layered WS_2 nanotubes [16], whereas the smallest inner core diameter would be ca. 0.4–1.2 nm with a 6.2 Å d-spacing [17,18]. It has been reported that MWCNs are capable of acting as templates for the generation of metal oxide thin layers [19]. In this Letter, we use MWCNs as a substrate on which thin layers of WO_3 are deposited, usually unevenly. These layers are then converted into ordered WS_2 by H_2S pyrolysis. Single- or multi-layered WS_2, either partly or fully coating the MWCNs, were produced according to HRTEM and EDX analyses. Here we present the results of detailed structural studies made on MWCNs partly coated by a single-layer of WS_2. The preparation of WO_3-coated MWCNs and the $WO_3 \rightarrow WS_2$ conversion procedure have been described elsewhere [20].

2. Results and discussion

A typical HRTEM result is shown in Fig. 1a, in which several features are distinguishable: (a) the WS_2 coating, verified by EDX, shows a fringe which is darker than the layers of carbon; (b) the WS_2 coating is cylindrical and the MWCN has eight shells; (c) the spacing between the WS_2 and the adjacent C layer is ca. 4.4 Å; (d) amorphous WO_3 (arrows) is also present on the tube surface, due to incomplete $WO_3 \rightarrow WS_2$ conversion (revealed by EDX); (e) the amorphous WO_3 coating is irregular and ca. 0.5–1.0 nm thick; (f) the basal-plane fringes within the carbon nanotube (CNT) core are not observed in the coated regions. We highlight the local structures (Fig. 1a) in order to study the relationship between the MWCN and the outer WS_2 coating. Fig. 1b and c show specific regions of the uncoated-CNT, to which we draw attention. The MWCN contains three compartments: C_1 and C_2 near to the C-tube tip (Fig. 1b) and C_3 close to the WS_2 coating (Fig. 1c). The relative volume of the three compartments is

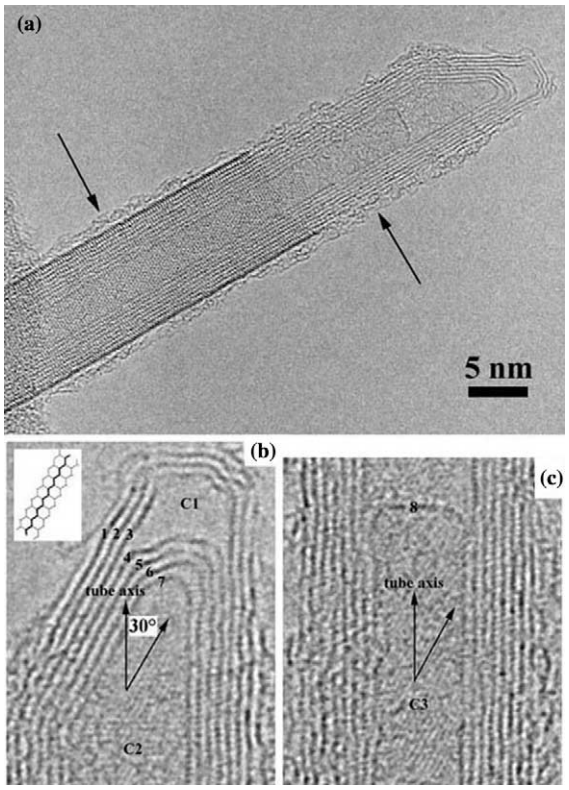

Fig. 1. (a) HRTEM image of a WS_2 partly-coated MWCN. (b) MWCN tip containing compartments C_1 and C_2. Insert: zigzag edge. (c) MWCN containing compartment C_3, near to the WS_2 coated region.

$C_3 > C_2 > C_1$. Compartment C_1 is fenced, somewhat imperfectly, by three outer and four inner layers, respectively. No clear fringes are visible within compartment C_1. Straight-line fringes, tilted at ca. 30° to the tube axis (arrows), together with weak amorphous-like fringes, are present within compartment C_2. When the straight-line fringes (30° tilted arrow, Fig. 1b) are enhanced by computer, very weak hexagonal-like patterns become visible. These linear fringes are consistent with the zigzag edge (insert, Fig. 1b). The amorphous material on the uncoated portion of the carbon nanotube possibly arises from the amorphous WO_3 coating (arrows, Fig. 1a) rather than from amorphous carbon deposited during MWCN preparation. Compartment C_3 also exhibits the same linear fringes (30° tilted arrow, Fig. 1c) as seen in compartment C_2. Based on Fig. 1b and c, we conclude that the linear fringes (i.e. zigzag fringes) arise from the carbon layers exhibiting the same chirality, possibly constituting the armchair edges (zigzag $\pm$ 30° = armchair). First, the compartment C_1 does not show linear fringes, implying that the chiralities differ in layers 1–3, however one or more of the layers fencing compartment C_1 may contribute to fringe formation in C_2 and C_3. Second, compartments C_2 and C_3 possess the same structural fringes, indicating that layers 4–7 have contributed to the fringe formation within C_2 and C_3. Unfortunately, we were unable to determine the chirality of layer 8, due to interference arising from layers 1–7.

Fig. 2a shows a diffractogram derived from Fig. 1a. This was calculated from a Fourier Transform of the WS_2-coated region of Fig. 1a. In order to clarify the details, only the WS_2 spots are indexed (Fig. 2b), however the (0 0 0 2) carbon plane is observed as a streak extending across the center of the image (arrow A, Fig. 2b) and some faint $(1\,0\,\bar{1}\,0)$ carbon spots (joined together by a black dashed line) are visible outside the ring of WS_2 spots. Two horizontal spots (arrow B, Fig. 2b) arise from that part of the carbon tube which is inclined at ca. 30° with respect to arrow A. The horizontal spots spacing (arrow B) is ca. 0.21 nm, corresponding to an armchair edge of $(1\,0\,\bar{1}\,0)$, which is consistent with Fig. 1b, i.e. the C-tube is armchair-edged.

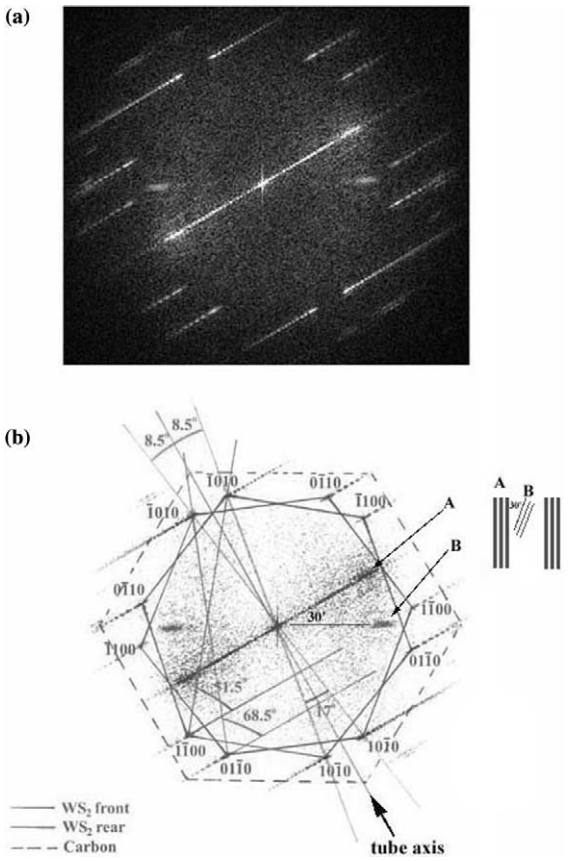

Fig. 2. (a) Diffractogram obtained from a Fourier transform of the WS_2-coated MWCN (Fig. 1a). (b) An indexed diffractogram. Note that the WS_2 front and rear spots have been labeled arbitrarily; it is not possible to distinguish the front and back layers without further tilting experiments.

Additionally, the following points can be made; (a) two sets of diffraction spots appear in hexagonal arrays, which match the diffraction pattern for the hexagonal WS_2 structure; (b) the two sets of hexagonal arrays result from the electron scattering by WS_2 as the TEM beam passes through the front and rear regions of the carbon nanotube, indicating that a single WS_2 layer is wrapped completely around the outer surface of the CNT to form a single-walled WS_2 nanotube coat; (c) the two hexagonal arrays are rotated away from each other by ca. 17° and are inclined at ca. 8.5° to the CNT axis. In other words, the WS_2 coating is a 8.5° helical tube. It is noteworthy that the streak

indicated by arrow A is a combination of the 3.4 Å C—C layers from the CNT and the single WS_2 layer. This conclusion is supported by the following observations. The CNT is coated with a single WS_2 layer only, therefore WS_2 (0 0 0 2) spots should be absent. In other words if no WS_2 layer were to be present at arrow A there would be two intense spots only, i.e. C(0 0 0 2), not a streak. The presence of a streak implies that a single WS_2 layer coats the CNT.

The WS_2 coating the MWCN terminates at different levels (white arrows, Fig. 3a). The hexagonal-like pattern is present between arrows, which corresponds to a single WS_2 sheet, as shown in Fig. 3b. First, dark spots, seen in Fig. 3a (between white arrows at the central core region), are regenerated, forming striation arrays (upper, Fig. 3b). Second, the regenerated spots are connected to form hexagonal rings (right, upper, Fig. 3b). Third, the hexagonal rings are then placed in a WS_2 sheet (lower, Fig. 3b) in order to locate W and S atoms. Fourth, the W atoms are arranged in hexagons with a single W atom located at the center (Fig. 3c). The S atoms are located in positions that would correspond to the hexagonal WS_2 structure. Several features may be distinguished as follows. (a) Individual spots (upper, Fig. 3b) correspond to W atoms, i.e. the TEM beam is mainly scattered by W atoms (b). The W–W distance is 3.1 Å, consistent with the WS_2 structure [21]. (c) Each row of hexagons is inclined at 8.5° with respect to the *a*-axis (arrow, upper Fig. 3b). (d) The straight-line fringes seen in compartments C_2 and C_3 do not interfere significantly with the WS_2 fringes. Based on points 1–4, we conclude that the hexagonal structure seen between the white arrows (Fig. 3a) is due to an extension of the WS_2 coating on the back of the CNT. The highlighted extended WS_2 coating is displayed in Fig. 3c. The hexagonal pattern is clearly present, and W and S atoms are located at the darker and weaker fringe sites, respectively. The inclination of the white arrow along the W—W edge is ca. 51.5° (Fig. 3c), which is consistent with the zigzag edge seen in Fig. 3b (arrow, lower) and the diffractogram (Fig. 2a and b). Meanwhile, the 8.5° inclined hexagonal rings are also consistent with the diffractogram (Fig. 2a and b).

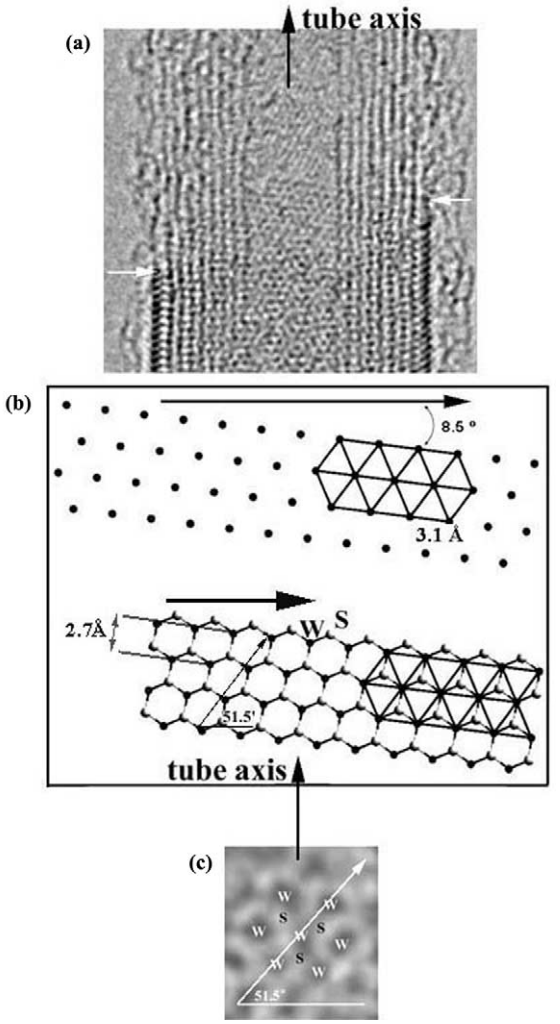

Fig. 3. (a) HRTEM image of WS_2—C interface; WS_2 terminating edges (white arrows). (b) Upper: simulated dark spot arrays from the excess of WS_2 coating at the rear of the tube (between white arrows, Fig. 2a); the W–W distance is 3.1 Å Lower: a simulated planar WS_2 structure where the W row separation distance is 2.7 Å. (c) Enhanced HRTEM image of WS_2 coating the rear of the MWCN (section between white arrows in Fig. 3a).

The hexagonal fringes become more complex and stronger below the white arrows (Fig. 3a), an effect consistent with constructive interference of signals from the rear and front surfaces of WS_2. In order to clarify the complex hexagonal structure seen in the WS_2 fully-coated area (Fig. 4a), a corresponding WS_2 tube has been simulated

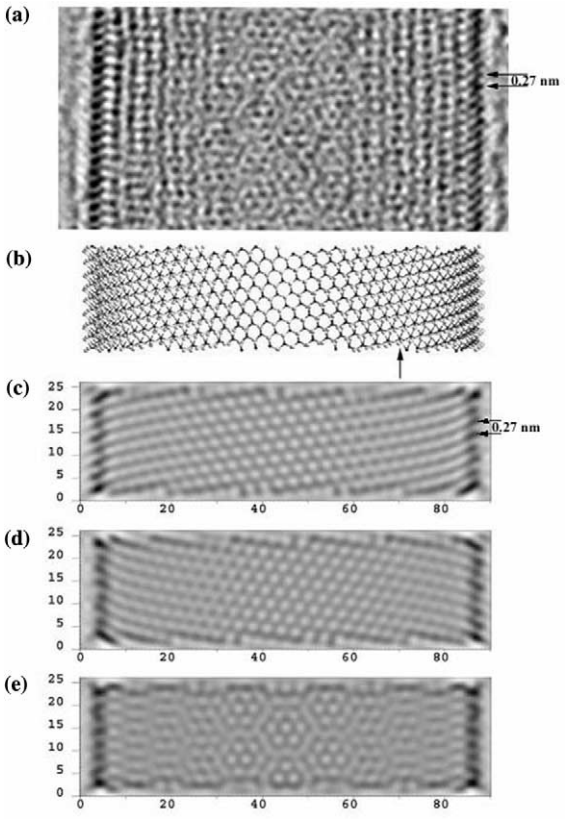

Fig. 4. (a) Enhanced TEM image of WS_2-coated area of Fig. 1a. Top right arrows indicate spacing (0.27 nm) between adjacent tadpole-like fringes, which is consistent with Fig. 3b (lower, small arrow) and Fig. 4c (arrows). (b) A simulated (90,−14) WS_2 tube. (c) Simulated HRTEM image for the front-half of a (90,−14) WS_2 tube ($E = 400$ kV, $C_s = 0.90$ mm, def $= -384.7$ Å, div $= 0.50$ mrad, Drms $= 100.0$ Å). (d) Simulated HRTEM image for the rear-half of a (90,−14) WS_2 tube. (e) Simulated HRTEM image for the whole (90,−14) WS_2 tube.

(Fig. 4b). The 8.5° helical WS_2 tube was constructed by rolling-up a WS_2 sheet along the (0,0) to (90,−14) vector. The diameter of a (90,−14) WS_2 nanotube is 8.42 nm, which is consistent with the 7.54 nm carbon nanotube outer-diameter and the 4.4 Å WS_2—C layer separation [20]. The simulated WS_2 tube was then bisected along its axis (Fig. 4b). HRTEM simulations were then performed for the front and rear halves (Fig. 4c and d), respectively. Several features are distinguishable: (a) The WS_2 hexagonal bonding structure is observed at the center of the simulated image, with W exhibiting a slightly darker contrast than S due to stronger electron beam scattering; (b) as the WS_2 layer curves away from the central section, darker spots appear, possibly due to the close relative positioning of W and S atoms perpendicular to the electron beam (arrow, Fig. 4b); (c) the darker spots begin to transform into continuous striations as the WS_2 layer curves towards the tube edges; (d) when the WS_2 layer lies parallel to the electron beam, WS_2 (0 0 0 2) side-wall fringes (tadpole-like) are produced; (e) each striation is separated by ca. 2.7 Å (arrows, Fig. 4a), which is consistent with estimates based on the WS_2 model (small arrow, lower Fig. 3b); (f) each striation slightly overlaps adjacent striations at the tube edges; (g) tadpole-like fringes are due to signals from several W and S atoms and therefore exhibit the strongest fringe contrast in the TEM image.

Complex hexagonal patterns are produced when front and rear halves are superimposed (central region, Fig. 4e), which is consistent with Fig. 4a. However, the shape of the tadpole fringes shown in Fig. 4a is similar to the front image (Fig. 4c), rather than the rear half image (Fig. 4d), which is due to the tube being tilted slightly. The indeterminate chirality in the C-layer 1 (i.e. the outermost layer) unfortunately makes the interface relationship between the WS_2 coating and C tubule difficult to explore [19].

Acknowledgements

We thank the Leverhulme Trust, the EPSRC and the Royal Society (UK) for financial support and D. Randall and J. Thorpe (University of Sussex) for contributions to TEM analysis.

References

[1] A. Thess, R. Lee, P. Nikolaev, H.J. Dai, P. Petit, J. Robert, C.H. Xu, Y.H. Lee, S.G. Kim, A.G. Rinzler, D.T. Colbert, G.E. Scuseria, D. Tomanek, J.E. Fischer, R.E. Smalley, Science 273 (1996) 483.
[2] J.W.G. Wildšer, L.C. Venema, A.G. Rinzler, R.E. Smalley, C. Dekker, Nature 391 (1988) 59.
[3] T.W. Odom, J.L. Huang, Ph. Kim, C.M. Lieber, Nature 391 (1998) 62.

[4] S. Iijima, J. Cryst. Growth 50 (1980) 675.
[5] S. Iijima, Nature 354 (1991) 56.
[6] M. Bretz, B.G. Demczyk, L. Zhang, J. Cryst. Growth 141 (1994) 304.
[7] X.F. Zhang, X.B. Zhang, G. VanTendeloo, S. Amelinckx, M.O. DeBeeck, VanLanduyt, J. Cryst. Growth 130 (1993) 368.
[8] M.Q. Liu, J.M. Cowley, Ultramicroscopy 53 (1994) 333.
[9] B.W. Smith, M. Monthioux, D.E. Luzzi, Nature 396 (1998) 323.
[10] R. Tenne, L. Margulis, M. Genut, G. Hodes, Nature 360 (1992) 444.
[11] W.K. Hsu, Y.Q. Zhu, S. Firth, R.J.H. Clark, H.W. Kroto, D.R.M. Walton, Adv. Fundam. Mater. 11 (2001) 69.
[12] W.K. Hsu et al., J. Am. Chem. Soc. 122 (2000) 10155.
[13] M. Remskar, Z. Skraba, P. Stadelmann, F. Levy, Adv. Mater. 12 (2000) 814.
[14] Y.Q. Zhu et al., J. Mater. Chem. 10 (2000) 2570.
[15] Y. Feldman, G.L. Frey, M. Homyonfer, V. Lyakhovitskaya, L. Margulis, H. Cohen, G. Hods, J.L. Hutchison, R. Tenne, J. Am. Chem. Soc. 118 (1996) 5362.
[16] M. Hershfinkel, L.A. Gheber, V. Volterra, J.L. Hutchison, L. Margulis, R. Tenne, J. Am. Chem. Soc. 116 (1994) 1914.
[17] L.C. Qin, X.L. Zhao, K. Hirahara, Y. Miyamoto, Y. Ando, S. Iijima, Nature 408 (2000) 50.
[18] N. Wang, Z.K. Tang, G.D. Li, S. Chen, Nature 408 (2000) 51.
[19] P.M. Ajayan, O. Stephan, Ph. Redlich, C. Colliex, Nature 375 (1995) 564.
[20] R.L.D. Whitby, W.K. Hsu, C.B. Boothroyd, P.K. Fearon, H.W. Kroto, D.R.M. Walton, Chem. Phys. Chem. 2 (2001) 620.
[21] The WS_2 lattice constant of 3.153 Å was obtained from reconstructing the WS_2 crystal from file JCPDS 8-237.